Stem Cell Reports, Volume *6*

Supplemental Information

Loss of *Asxl1* Alters Self-Renewal and Cell Fate of Bone Marrow Stromal Cell, Leading to Bohring-Opitz-like Syndrome in Mice

Peng Zhang, Caihong Xing, Steven D. Rhodes, Yongzheng He, Kai Deng, Zhaomin Li, Fuhong He, Caiying Zhu, Lihn Nguyen, Yuan Zhou, Shi Chen, Khalid S. Mohammad, Theresa A. Guise, Omar Abdel-Wahab, Mingjiang Xu, Qian-Fei Wang, and Feng-Chun Yang

Stem Cell Reports, Volume *6*

Supplemental Information

Loss of *Asxl1* Alters Self-Renewal and Cell Fate of Bone Marrow Stromal Cell, Leading to Bohring-Opitz-like Syndrome in Mice

Peng Zhang, Caihong Xing, Steven D. Rhodes, Yongzheng He, Kai Deng, Zhaomin Li, Fuhong He, Caiying Zhu, Lihn Nguyen, Yuan Zhou, Shi Chen, Khalid S. Mohammad, Theresa A. Guise, Omar Abdel-Wahab, Mingjiang Xu, Qian-Fei Wang, and Feng-Chun Yang

Inventory of Supplemental Information

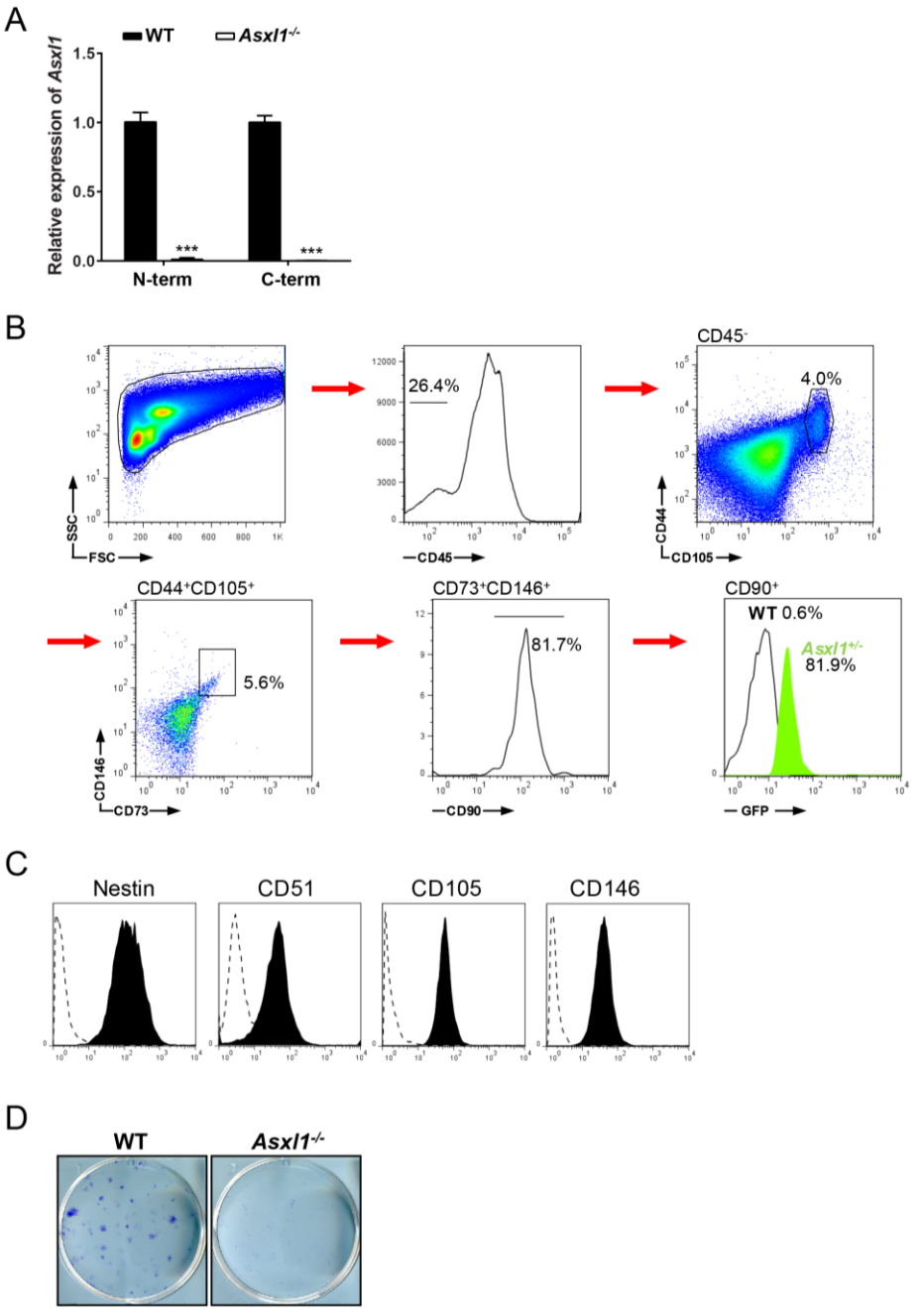

Figure S1. Related to Figure 1 and Figure 2. (A) qPCR shows the expression level of *Asxl1* in WT and *Asxl1*$^{-/-}$ BMSCs (n=7 mice per genotype). N-term and C-term indicate the position of primers used. (B) Representative flow cytometry plots show the population of BMSCs in the bone marrow of WT and *Asxl1*$^{+/-}$ mice. (C) Representative flow cytometric analysis of clonal non-adherent mesenspheres cultured from BMSCs. (D) A representative photomicrograph of CFU-F from WT and *Asxl1*$^{-/-}$ BMSCs, after staining with the HEMA-3 Quick Staining Kit.

Data are presented as mean ± SEM. ***$p < 0.001$.

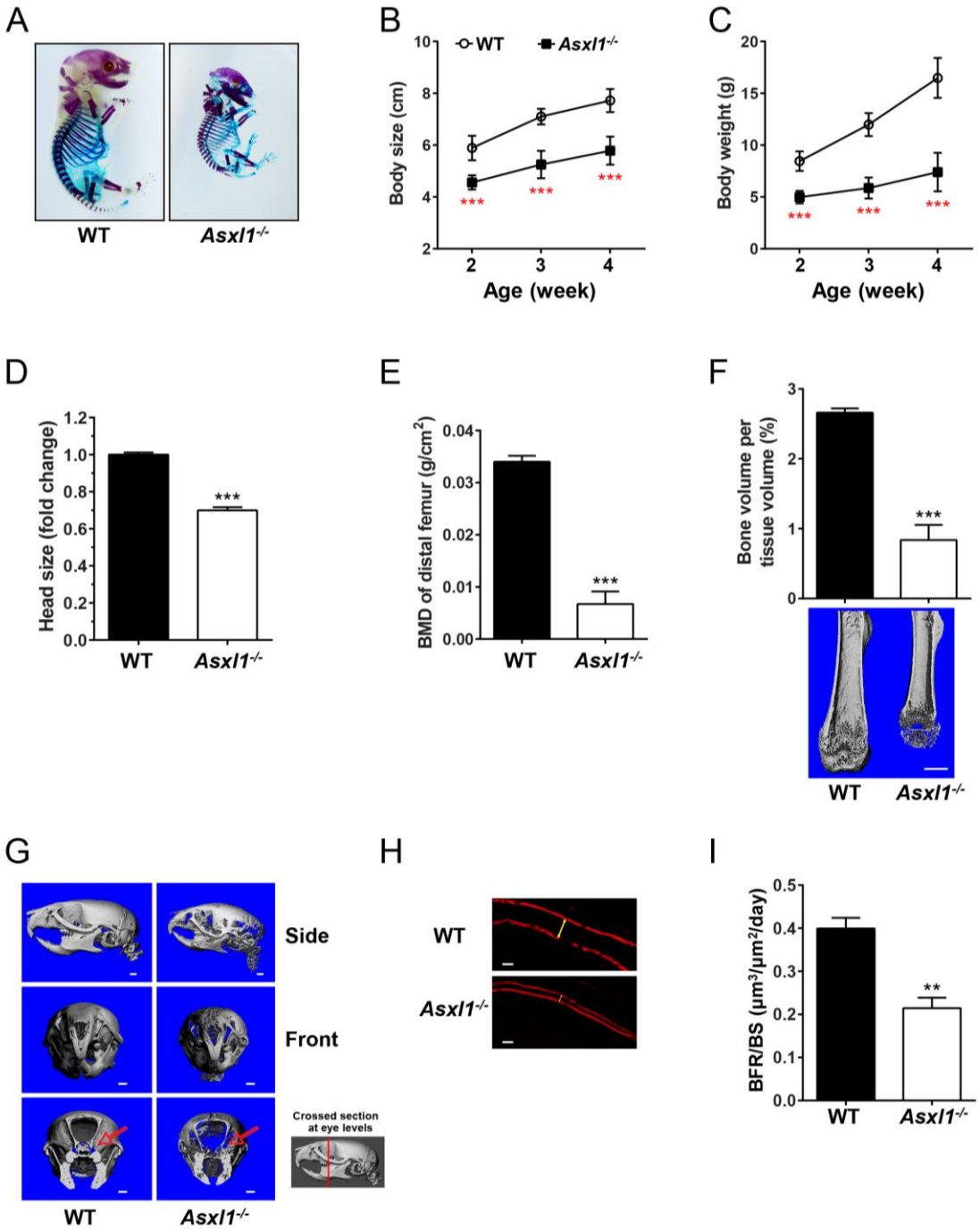

Figure S2. Related to Figure 3. (A) Whole-mount skeletal staining on embryonic day 18.5 shows reduced body size and characteristic eye defects in *Asxl1*$^{-/-}$ embryos compared with WT. (B-C) Serial measurements of body length (B) and weight (C) in WT and *Asxl1*$^{-/-}$ mice (n=12 mice per genotype) are shown. Mice were measured and weighed weekly at the same time. (D) Head size of *Asxl1*$^{-/-}$ mice, measured via X-ray images, is significantly smaller than WT mice (WT, n=12 mice; *Asxl1*$^{-/-}$ n=9 mice). (E) BMD of the distal femur was determined by pDEXA 3

weeks after birth. The *Asxl1*$^{-/-}$ mice exhibit significantly reduced BMD compared with WT littermates (n=14 mice per genotype). (F) µCT analysis of femurs from 3-week-old *Asxl1*$^{-/-}$ mice and WT littermates (n=5 mice per genotype). Bone volume is significantly decreased in *Asxl1*$^{-/-}$ mice. Representative µCT reconstructed femurs are shown for WT versus *Asxl1*$^{-/-}$ mice. Scale bar represents 1 mm. (G) Developmental abnormalities of the *Asxl1*$^{-/-}$ skull (upper) and eye (lower) are shown in representative µCT scans. Scale bar represents 1 mm. (H-I) Dynamic bone histomorphometry was preformed using alizarin labelling (H). The bone formation rate (BFR/BS, I) was significantly decreased in *Asxl1*$^{-/-}$ mice compared with WT littermates (n=3 mice per genotype). Scale bars represent 20 µm.

Data are presented as mean ± SEM. **$p < 0.005$, ***$p < 0.001$.

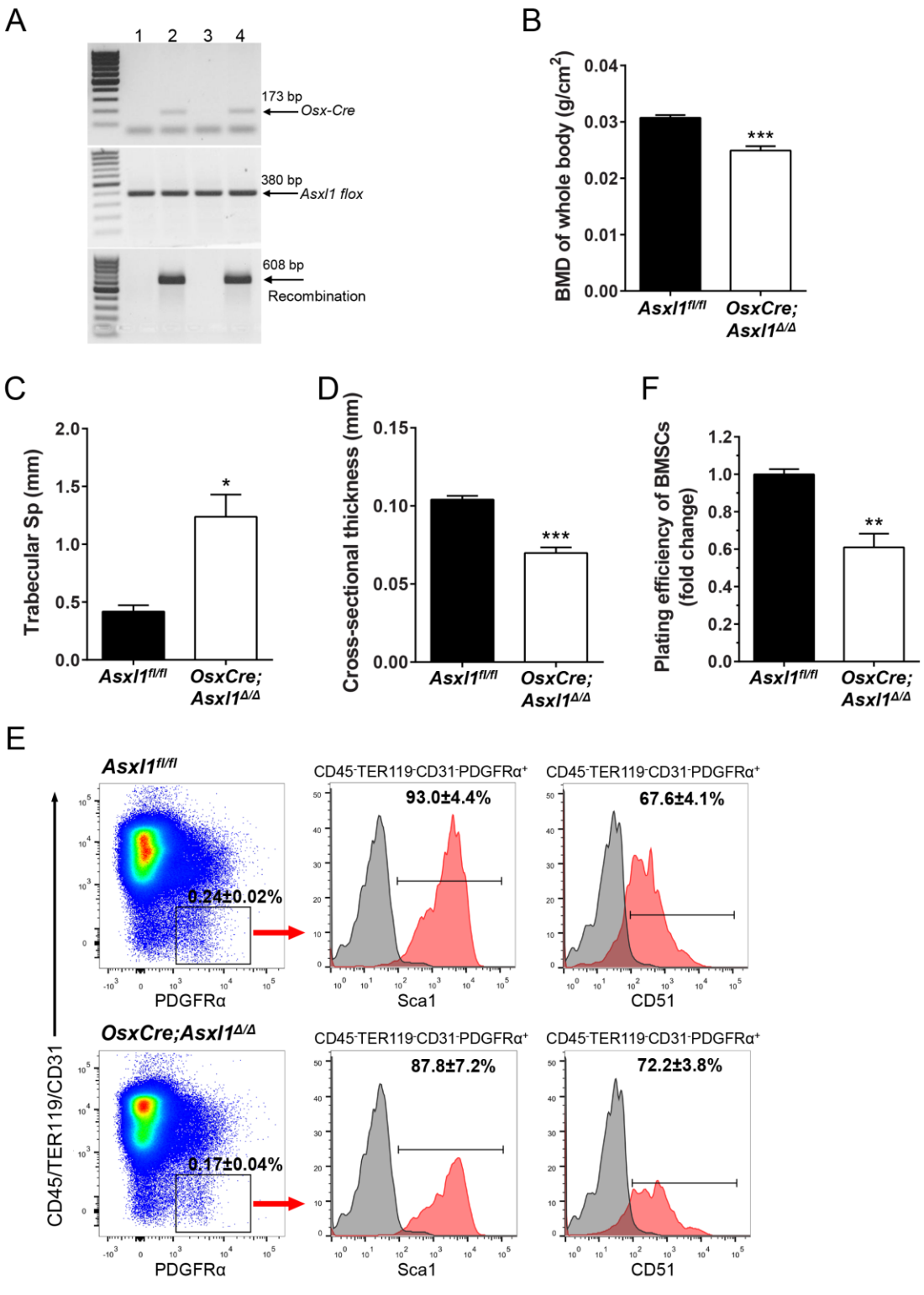

Figure S3. Related to Figure 3. (A) PCR genotyping of *OsxCre;Asxl1*$^{\Delta/\Delta}$ mice and *Asxl1*$^{fl/fl}$ littermates. DNA templates used for PCR analysis were obtained from mouse toes. Bottom PCR

shows the presence of a recombination band in *OsxCre;Asxl1*$^{\Delta/\Delta}$ mice, but not in *Asxl1*$^{fl/fl}$ littermates. (B) Whole body BMD of *OsxCre;Asxl1*$^{\Delta/\Delta}$ (n=6 mice) is significantly reduced compared with controls (n=4 mice). (C) µCT analysis of trabecular spacing in the femurs of *OsxCre;Asxl1*$^{\Delta/\Delta}$ (n=6 mice) and *Asxl1*$^{fl/fl}$ littermates (n=4 mice). (D) Cross-sectional cortical bone thickness of the femur midshaft is significantly decreased in *OsxCre;Asxl1*$^{\Delta/\Delta}$ (n=6 mice) compared with *Asxl1*$^{fl/fl}$ littermates (n=4 mice). (E) Representative flow cytometry plots show the population of PDGDRα^{+} BMSCs and the marker expression in the bone marrow of *OsxCre;Asxl1*$^{\Delta/\Delta}$ mice and littermate controls. n=4-6 mice from three independent experiments. (F) Plating efficiency of BMSCs from *OsxCre;Asxl1*$^{\Delta/\Delta}$ mice and *Asxl1*$^{fl/fl}$ littermates (n=4 mice per genotype).

Data are presented as mean ± SEM. *$p < 0.05$, **$p < 0.005$, ***$p < 0.001$.

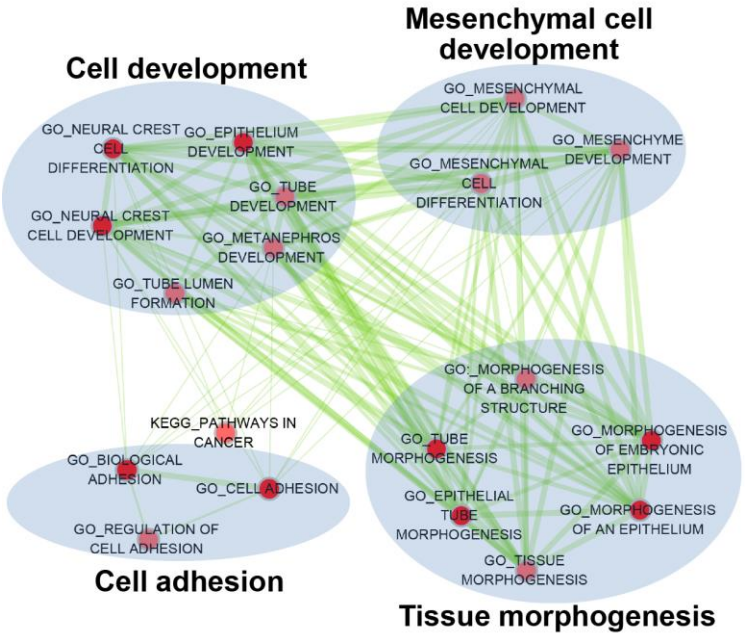

Figure S4. Related to Figure 4. Enrichment map was used for visualizing the network of KEGG pathways and GO terms enriched with up-regulated genes in *Asxl1*$^{-/-}$ BMSCs. Nodes and ovals indicate enriched functional gene sets ($p < 0.01$ and FDR < 0.25 in DAVID) and functional clusters, respectively. Edges indicate overlap between the enriched gene-sets; thickness represents significance. Only edges with a Fisher's exact test nominal p value smaller than 10^{-4} were visualized. Color intensity is proportional to enrichment significance.

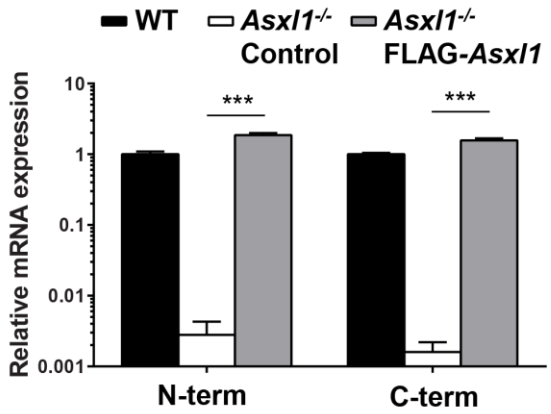

Figure S5. Related to Figure 5. qPCR shows the expression level of *Asxl1* mRNA in *Asxl1*$^{-/-}$ BMSCs rescued by transduction of FLAG-*Asxl1* from five independent experiments. N-term and C-term indicate the position of primers used.

Data are presented as mean ± SEM. ***$p < 0.001$.

Table S1. Primers used for qPCR.

Primer name	Primer Sequence (5'-3')	Product (bp)	Reference
Asxl1-F1 (N-term)	TCTACAGAGTCTCAGAGCCG	98	
Asxl1-R1 (N-term)	AGCATAACCCCAGTCCTTTTC		
Asxl1-F2 (C-term)	TCACACCGAAAAGCCACAG	120	
Asxl1-R2 (C-term)	GGGCATATCTGGTAAGTGGG		
Nanog-F1	AGGGTCTGCTACTGAGATGCTCTG	364	(Chen et al., 2006)
Nanog-R1	CAACCACTGGTTTTTCTGCCACCG		
Pou5f1-F1	CTGTAGGGAGGGCTTCGGGCACTT	485	(Chen et al., 2006)
Pou5f1-R1	CTGAGGGCCAGGCAGGAGCACGAG		
Sox2-F	ACAAGAGAATTGGGAGGGGT	120	
Sox2-R	TTTTCTAGTCGGCATCACCG		
Actb-F	GGCTGTATTCCCCTCCATCG	154	
Actb-R	CCAGTTGGTAACAATGCCATGT		
Runx2-F	ACACCGTGTCAGCAAAGC	99	
Runx2-R	GCTCACGTCGCTCATCTTG		
Bglap1-F	GGTAGTGAACAGACTCCGGC	96	
Bglap1-R	CAAGCAGGGTTAAGCTCACA		
Sp7-F	GATGGCGTCCTCTCTGCTT	146	
Sp7-R	CGTATGGCTTCTTTGTGCCT		
Alpl-F	ACTGCGCTCCTTAGGGCT	104	
Alpl-R	GGCAGCGTCAGATGTTAATTG		
Pparγ-F	GATGCACTGCCTATGAGCAC	110	
Pparγ-R	TCTTCCATCACGGAGAGGTC		
Cebpα-F	CCAAGAAGTCGGTGGACAAG	95	
Cebpα-R	TTGTTTGGCTTTATCTCGGC		
Fabp4-F	AATGTGTGATGCCTTTGTGG	100	
Fabp4-R	CACTTTCCTTGTGGCAAAGC		
Lpl-F	TTTGGCTCCAGAGTTTGACC	110	
Lpl-R	TGTGTCTTCAGGGGTCCTTAG		

Table S2. Antibodies used for western blot.

Antibodies	Catalogue Number
NANOG	Cell Signaling 8600
OCT4 (N-19)	Santa Cruz sc-8628
SOX2	Abcam ab59776
β-ACTIN	Sigma A2228
M2-FLAG	Sigma F3165

Supplemental Experimental Procedures

Chemicals were obtained from Sigma (St. Louis, MO) unless otherwise indicated.

ASXL1 Murine Models

The generation of *Asxl1:nlacZ/nGFP* knock-in and *Asxl1*$^{fl/fl}$ mice has been previously described (Abdel-Wahab et al., 2013; Wang et al., 2014). Heterozygous *Asxl1:nlacZ/nGFP* (*Asxl1*$^{+/-}$) mice were interbred to obtain homozygous *Asxl1:nlacZ/nGFP* (*Asxl1*$^{-/-}$) mice. *Osx-Cre* transgenic mice were purchased from Jackson Laboratories. All mice were bred on a C57BL/6 genetic background. All protocols were approved by the Institutional Animal Care and Use Committee at University of Miami Miller School of Medicine.

X-Ray, Peripheral Dual-Energy X-Ray Absorptiometry (pDEXA), and Micro-Computed Tomography (µCT)

The mice were anesthetized with ketamine (150 mg/kg) administered by intraperitoneal (IP) injection and placed in the lateral position in an XPERT 80 Digital Cabinet X-ray System (Kubtec, Milford, CT). Radiographs were acquired to demonstrate the size difference between WT and *Asxl1*$^{-/-}$ mice.

Bone mineral density (BMD) was measured by pDEXA with a Lunar Piximus densitometer (GE Medical Systems, software version 1.4 Lunar) (Yang et al., 2006). The mice were anesthetized and placed into the scanner in the prone position with arms and legs extended. The head was excluded from total body scans. The BMD of the left femoral metaphysis was measured by defining a region of interest of 12 pixels x 12 pixels proximal to the distal growth plate, a region containing a high content of trabecular bone.

Bone volume and microarchitecture in the distal femoral metaphysis were evaluated using a high-resolution desktop µCT imaging system (VivaCT 40; Scanco Medical AG, Basserdorf, Switzerland) (Rhodes et al., 2013). Scanning for the femur was started at 15% of the total femur length measured from the tip of femoral condyle and extending proximally for 200 slices with an increment of 9 µm, which were then reconstructed, filtered (σ=0.8 and support=1.0), and thresholded (at 16% of the possible gray scale value) for analysis (Munugalavadla et al., 2008). The area for trabecular analysis was outlined within the trabecular compartment, excluding the cortical and subcortical bone. Every 10 sections were outlined manually, and the intermediate sections were interpolated with the contouring algorithm to create a volume of interest.

Parameters of microarchitecture for both skeletal sites included bone volume (BV, mm^3), bone volume fraction (BV/TV, %), trabecular number (Tb.N, mm^{-1}), trabecular thickness (Tb.Th, mm), and trabecular spacing (Tb.Sp, mm).

Fluorochrome Bone Labeling

Fluorochrome labeling of the bones was performed in 3-week old mice by intraperitoneal injections of alizarin (20 mg/kg, Sigma) 8 and 3 days before sacrifice, as previously described (Warden et al., 2005; Wu et al., 2011). After sacrifice, femurs were fixed in 10% neutral buffered formalin for 48 hours, dehydrated in graded ethanols, and embedded undecalcified in methylmethacrylate.

Frontal sections (4 mm thick) were cut from the distal femur using a motorized microtome equipped with a tungsten-carbide knife (Leica Inc, Deerfield IL). The sections were mounted unstained for fluorochrome-derived bone formation parameters. Trabecular bone turnover was assessed by measuring the extent of single label (sL.Pm), double label (dL.Pm) and the area of bone (dL.Ar) between double alizarin labels using Image Pro Plus version 4.1 software (MediaCybernetics, Silver Spring, MD). Derived histomorphometric parameters included mineralizing surface (MS/BS, %), a measure of active bone-forming surface, calculated as follows: the [KsL.Pm+dL.Pm]/Tt.Pm * 100; mineral apposition rate (MAR, μm/day), a measure of the rate of radial expansion of new bone, calculated as follows: dL.Ar/dL.Pm/4 dy; and bone formation rate, an overall measure of bone formation that combines MS/BS and MAR, calculated as follows: MS/BS * MAR.

Flow Cytometry

Bone marrow stromal cell (BMSC) populations were delineated *in vivo* by evaluating the expression of surface markers by flow cytometry on a FACSCalibur. Antibodies for flow cytometry were purchased from BD-Pharmingen and BioLegend. BMSCs were stained with antibodies against CD146 (PE), CD105 (APC), CD45 (PerCP), CD44 (PE-Cy7), CD90 (APC-Cy7), and CD73 (PacBlue), or antibodies against PDGFRα (APC), CD51 (PE), Sca1 (PE-Cy7), CD45 (FITC), TER119 (FITC), and CD31 (FITC). Following incubation of cells with antibodies for 30 minutes at 4°C, cells were washed 3 times with PBS containing 0.1% bovine serum albumin (BSA) and analyzed using a FACSCalibur instrument (Becton Dickinson).

BMSC Culture and Lineage Differentiation Assays

To measure the frequency of BMSCs in bone marrow, the colony forming unit fibroblast (CFU-F) assay was performed as previously described (Wu et al., 2006). Briefly, $4x10^6$ of bone marrow mononuclear cells (BMMNCs) were plated into 6-well tissue culture plates in triplicate for each condition in mouse MesenCult medium (MesenCult basal media plus 20% of MesenCult Supplemental, Stem Cell Technologies Inc,) and incubated at 37°C and 5% CO_2. After 14 days of culture, medium was removed and each well was washed with phosphate-buffered saline (PBS), stained with a HEMA-3 quick staining kit (Fisher Scientific Company, VA, USA) according to the manufacturer's instructions and photographed.

For CFU-osteoblast assays, after 7 days of culture, medium was removed and switched to osteogenic differentiation medium (MesenCult medium supplemented with 10^{-7} M dexamethasone, 50 μg/mL ascorbic acid and 10 mM β-glycerophosphate). Medium was changed every other day for one week of continuous culture. Staining for ALP activity was subsequently performed using a Leukocyte Alkaline Phosphatase kit according to the manufacturer's instructions. Photomicrographs of the stained cells were acquired with a Nikon TE2000-S microscope. The area and intensity of ALP^+ cells were quantified using Image J software.

For CFU-adipocyte assays, after 5 days of culture, medium was changed to adipogenic differentiation medium (MesenCult medium supplemented with 10^{-7} M dexamethasone, 450 μM isobutylmethylxanthine, 1 μg/ mL insulin and 200 μM indomethacin). Culture medium was changed every 5 days for 4 weeks. Adipocytes were determined with Oil Red O staining.

BMSCs were generated from each experimental group of mice as previously described (Wu et al., 2006). Briefly, BMMNCs were separated by low density gradient centrifugation from 3- to 4-week old mice, and then resuspended and cultured in mouse MesenCult medium at 37°C and 5% CO_2. When the cultures reached 80 to 90% confluency, cells were trypsinized and replated. BMSCs of identical passage number (between passages 3 to 5) were used for experiments.

For osteoblast differentiation, $5x10^4$ BMSCs were cultured for 7 days in 6-well plates using osteogenic differentiation medium. To induce adipocyte differentiation *in vitro*, $1x10^5$ BMSCs were plated in 6-well tissue culture plates and cultured with adipogenic differentiation medium. For chondrocyte differentiation assays, $1x10^5$ BMSCs were plated in 6-well plates and cultured with chondrogenic differentiation medium (osteogenic differentiation medium supplemented with 10 ng/mL TGFβ3).

Mesensphere Assays

For clonal mesensphere formation, BMSCs were plated at clonal density (~1,000 cells cm^2) in ultralow adherent 24-well plates (Corning) as previously described (Mendez-Ferrer et al., 2010; Pinho et al., 2013). The growth medium contained 15% chicken embryo extract (Fisher Scientific), 0.1 mM β-mercaptoethanol, 1% non-essential amino acids, 1% N2 and 2% B27 supplements (Gibco), fibroblast growth factor (FGF)-basic, insulin-like growth factor-1 (IGF-1), epidermal growth factor (EGF), platelet-derived growth factor (PDGF) and oncostatin M (OSM) (Peprotech) (20 ng/mL) in DMEM/F12 (1:1)/human endothelial (Gibco) (1:2). The cultures were maintained at 37°C in a 5% CO_2, water-jacketed incubator and left untouched for 1 week to prevent cell aggregation in low density cultures. Half of the medium was changed weekly. The mesensphere colonies were detached with trypsin, and the cells were mechanically dispersed and re-plated back into ultralow adherent plates with culture medium. Secondary mesenspheres were counted after 7 days in culture.

Proliferation Assays

Cell proliferation was examined by the [^{3}H] thymidine incorporation assay as previously described (Wu et al., 2006). Briefly, $5x10^3$ WT or *Asxl1*$^{-/-}$ BMSCs were plated in 96-well flat-bottom plates in 100 μL MesenCult medium in a 37°C and 5% CO_2, humidified incubator overnight. The cells were starved with 100 μL α-MEM medium (Gibco) without supplements for 24 hours, and then cultured in MesenCult medium for 24 hours, and [^{3}H] thymidine was added to cultures 6 hours before harvest with an automated 96-well cell harvester (Brandel, Gaithersburg, MD). γ-Emission was measured with a microplate scintillation counter (PerkinElmer Life and Analytical Sciences, Boston, MA). Assays were performed in triplicate.

Generation of Stably *Asxl1*-Transduced BMSCs

The full-length mouse *Asxl1* cDNA with an N-terminal FLAG tag was cloned, and then subcloned into the lentiviral vector with *Xho*I and *Nhe*I double digestion and ligation. The empty vector was used for control. All constructs were validated by direct sequencing prior to lentiviral generation. Recombinant lentiviral vectors were produced in HEK293T cells using the helper plasmid pCD/NL-BH and the VSV-G envelope plasmid. Lentivirus containing supernatants were concentrated and tittered. BMSCs were split approximately 16 hours prior to transduction and

then transduced overnight with concentrated supernatants resuspended in MesenCult medium. Medium was replaced the next day and transduced cells were cultured and expanded. $EGFP^+$ cells were sorted using a FACS Vantage flow cytometer. Before further experiments, transduction and selection efficiency were verified by qPCR and western blot analysis.

Gene Expression Analysis by qPCR and RNA-Seq

Genes of interest mRNA levels were determined by real-time qPCR. Total RNA was extracted with TRIzol reagent (Ambion). qPCR was performed in triplicate using an ABI 7500 with SYBR green PCR kits (Applied Biosystems). mRNA levels were normalized to housekeeping gene *β-actin* expression. All qPCR primers used are listed in Table S1.

For RNA-seq, mRNA library preparation was performed with the Illumina TruSeq strand specific mRNA sample preparation system (Illumina). Briefly, mRNA was extracted from total RNA using polyA selection, followed by RNA fragmentation. A strand specific library was constructed by first-strand cDNA synthesis using random primers, sample cleanup and second-strand synthesis using DNA polymerase I and RNase H. A single 'A' base was added to the cDNA fragments followed by ligation of the adapters. A final cDNA library was achieved by further purification and enrichment with PCR, with quality checked using the Agilent 2100 Bioanalyzer. The library was sequenced (PE100bp) using the Illumina HiSeq2500, with 4 samples per lane, and final of over 20 million reads per sample.

RNA-seq reads were aligned to the mouse genome reference sequence (GRCm38/mm10) using TopHat (Trapnell et al., 2012) with a tolerance of two mismatches. Cuffdiff (Trapnell et al., 2012) was used to detect the differentially expressed genes with cutoff of $p < 0.05$ and false discovery rate (FDR) < 0.25. The identified differentially expressed genes were used for pathway enrichment analysis and functional annotation with the Database for Annotation, Visualization and Integrated Discovery (DAVID) Bioinformatics resources (Huang da et al., 2009). A heatmap was generated in R using the gplot package. GSEA analysis (Subramanian et al., 2005) was performed in MSigDB (http://www.broadinstitute.org/gsea/msigdb/index.jsp) to generate the list of the most differentially expressed genes, including Kyoto Encyclopedia of Genes and Genomes (KEGG) pathway signatures and stem cell signatures. Enriched gene sets were selected using a cut-off of $p < 0.05$ and FDR < 0.25 (Isserlin et al., 2014).

Western Blot Analysis

BMSC cell lysates were subjected to western blot analysis. Isolated proteins were fractionated using NuPAGE 4-12% Bis-Tris Gels (Invitrogen) and electro-transferred to PVDF membranes (Roche). Immunoblots were performed using specific antibodies (Table S2). After incubation with anti-rabbit IgG or anti-mouse IgG (GE Healthcare) antibodies conjugated with HRP, signals were detected using ECL chemiluminescence substrate (Pierce).

Statistical Analysis

Differences between experimental groups were determined by Student's *t*-test or ANOVA followed by Newman-Keuls multiple comparison tests as appropriate. p values of less than 0.05 were considered significant.

Supplemental References

Chen, S., Do, J.T., Zhang, Q., Yao, S., Yan, F., Peters, E.C., Scholer, H.R., Schultz, P.G., and Ding, S. (2006). Self-renewal of embryonic stem cells by a small molecule. Proceedings of the National Academy of Sciences of the United States of America *103*, 17266-17271.

Munugalavadla, V., Vemula, S., Sims, E.C., Krishnan, S., Chen, S., Yan, J., Li, H., Niziolek, P.J., Takemoto, C., Robling, A.G., *et al.* (2008). The p85alpha subunit of class IA phosphatidylinositol 3-kinase regulates the expression of multiple genes involved in osteoclast maturation and migration. Molecular and cellular biology *28*, 7182-7198.

Rhodes, S.D., Wu, X., He, Y., Chen, S., Yang, H., Staser, K.W., Wang, J., Zhang, P., Jiang, C., Yokota, H., *et al.* (2013). Hyperactive transforming growth factor-beta1 signaling potentiates skeletal defects in a neurofibromatosis type 1 mouse model. Journal of bone and mineral research : the official journal of the American Society for Bone and Mineral Research *28*, 2476-2489.

Yang, F.C., Chen, S., Robling, A.G., Yu, X., Nebesio, T.D., Yan, J., Morgan, T., Li, X., Yuan, J., Hock, J., *et al.* (2006). Hyperactivation of p21ras and PI3K cooperate to alter murine and human neurofibromatosis type 1-haploinsufficient osteoclast functions. The Journal of clinical investigation *116*, 2880-2891.